Model of high-order harmonic generation from laser interaction with a plasma grating

S. J. Zhang,[1] H. B. Zhuo,[1,2,*] D. B. Zou,[1,†] L. F. Gan,[1] H. Y. Zhou,[1] X. Z. Li,[1] M. Y. Yu,[3] and W. Yu[4]

[1]*College of Science, National University of Defense Technology, Changsha 410073, P. R. China*

[2]*IFSA Collaborative Innovation Center, Shanghai Jiao Tong University, Shanghai 200240, P. R. China*

[3]*Institute for Fusion Theory and Simulation, Zhejiang University, Hangzhou 310027, P. R. China*

[4]*Shanghai Institute of Optics and Fine Mechanics, Chinese Academy of Sciences, Shanghai 201800, P. R. China*

(Received 26 February 2016; published 23 May 2016)

Harmonic generation from linearly polarized high-intensity short-pulse laser normally impacting a solid plasma grating is investigated using analytical modeling and particle-in-cell simulation. It is found that when the radiation excited by the relativistic electron quiver motion in the laser fields suitably matches a harmonic of the grating periodicity, it will be significantly enhanced and peak with narrow angular spread in specific directions. The corresponding theory shows that the phenomenon can be attributed to an interference effect of the periodic grating on the excitation.

DOI: 10.1103/PhysRevE.93.053206

High-order harmonic generation (HHG) from laser plasma interaction is promising as an efficient source for extreme ultra-violet (XUV) and attosecond pulses [1–3]. The physics involved is of basic interest and the resulting radiation are relevant for applications in many areas [4–6]. Two dominant HHG mechanisms have now been clearly identified on flat solid plasma irradiated by relativistic laser pulse, including the coherent wake emission [7] and the relativistic oscillating mirror process [8,9]. The plasma here acts as a mirror to the incident field, leading to a periodic temporal distortion of the reflected waveform and thus the harmonic generation in the specular reflection of the laser pulse. Powerful HHG with a quite different characteristics has also been observed in experiment from the grating surface normally irradiated by a linearly laser pulse [10]. The results showed that only the harmonics of the grating periodicity were strongly generated, which is emitted along the surface direction with a narrow solid angle. Indicated by the related numerical studies [11,12], such HHG is attributed to the relativistic dynamic of electron bunches coming from the corrugated surface, meanwhile the diffractive prosperities of grating play important roles in spectrum and angular distribution of the emission. However, a satisfactory physical understanding of the HHG on the grating plasma is still lacking.

In this paper, we propose an analytical surface-current model for investigating HHG when a relativistic *linearly polarized* laser pulse incidents *normally* on a solid plasma grating. It is found that the relativistic quiver motion of teeth electrons in the laser light leads to HHG. Due to the interference effect of the grating, harmonics that suitably match the harmonic of the grating periodicity are greatly amplified and folded into a narrow solid angle nearly parallel to the surface. Both the HHG spectrum and the angular distribution obtained from two-dimensional (2D) particle-in-cell (PIC) simulation are consistent with that from the analytical results.

Consider a linearly polarized ultrashort laser pulse normally impinging on a plasma grating surface, as shown in Fig. 1. We simply assume that the grating structure does not vary significantly within the ultrashort interaction time and the tooth profile roughly remains steplike. Thus the plasma density of tooth is n_0 for $z < 0$ and zero for $z \geqslant 0$. At the vacuum-tooth plasma interface, the boundary condition is $H_t(0,t) = 2H_i(0,t)$, where H_i and H_t are the magnetic fields of the incident and transmitted waves, respectively. For the condition $w \ll \ell \ll \lambda_0$, where λ_0 is the laser wavelength, we can ignore the influence of the grating on the incident and transmitted field distribution. For large n_0, the transmitted wave can be represented by a surface current $j(t)$, so the boundary condition can be written as $(4\pi/c)j(t) = 2H_i(0,t)$ [13]. In the solid-density plasma considered here, we have $n_0 \gg n_c$, where n_c is the critical density, and the laser penetration is confined to an extremely small (say less than 1/10th the laser wavelength) region inside the plasma surface. One then obtains $\boldsymbol{j}(t) = (m_e\omega_0 c^2/2\pi e)\gamma\boldsymbol{\beta}(t)$, where $\gamma = (1-\beta^2)^{-1/2}$, $\boldsymbol{\beta} = \boldsymbol{v}/c$, $\boldsymbol{v}$ is the electron quiver velocity in the laser field, c is the speed of light, and ω_0 is the laser frequency.

The radiated power per unit solid angle of the nth harmonic from a current source consisting of the single tooth electrons moving relativistically in the linearly polarized laser field can be expressed as [13]

$$\frac{dP_n}{d\Omega} = \frac{n^2\omega_0^2}{8\pi^3 c^3}\left|\int d^3x \exp(-ink_0\hat{\boldsymbol{n}}\cdot\boldsymbol{x})\int_0^{2\pi} d\tau \boldsymbol{G}_n\right|^2, \quad (1)$$

where $\boldsymbol{G}_n = \hat{\boldsymbol{n}}\times(\hat{\boldsymbol{n}}\times\boldsymbol{j})\exp[in(\tau - k_0\hat{\boldsymbol{n}}\cdot\boldsymbol{\Delta})]$, $\hat{\boldsymbol{n}}$ is the direction of emission, $\boldsymbol{x}$ is the coordinate vector of the source at $\tau = 0$, $\boldsymbol{\Delta}(\boldsymbol{x},\tau) = \int_0^\tau v(\boldsymbol{x},\tau')d\tau'$ is its displacement, $\tau = \omega_0 t$, and $k_0 = \omega_0/c$. The instantaneous location of the oscillating electron is therefore at $\boldsymbol{x} + \boldsymbol{\Delta}$ [14].

For the normalized vector potential of the incident laser light of $\boldsymbol{a} = \hat{\boldsymbol{y}}a_0\exp[i(\tau + k_0 z)]$, it is convenient to define $\boldsymbol{\beta} = \hat{\boldsymbol{y}}\beta\cos\tau$, thus $\boldsymbol{\Delta} = \hat{y}\beta c/\omega_0\sin\tau$, where $\beta = a_0/(1+a_0^2)^{1/2}$. Substituting $\boldsymbol{\Delta}$, and $j(t)$ into Eq. (1), we obtain

$$\frac{dP_n}{d\Omega} = \left(\frac{\gamma m_e\omega_0 c}{2\pi e}\right)^2 K_n(\theta), \quad (2)$$

where θ is the observation angle in respect to $\hat{y}$. The radiation $K_n(\theta)$ from a single electron quivering (oscillating) in the

*hongbin.zhuo@gmail.com

†zoudebin@126.com

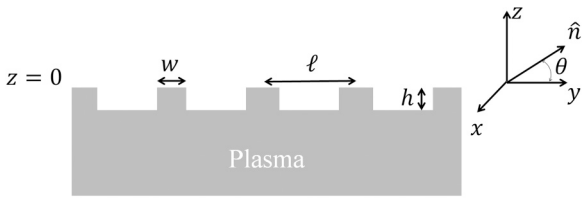

FIG. 1. Interaction configuration. The linearly laser beam incidents normally on the grating surface with its electric field polarized along the $\hat{y}$ axis. ℓ, h, and w are the grating periodicity and the height and width of the tooth, respectively. $z = 0$ is the interface of the tooth plasma and vacuum.

linearly laser field is [13]

$$K_n(\theta) = \frac{n^2 e^2 \omega_0^2}{2\pi c} \tan^2\theta J_n^2(n\beta\cos\theta). \tag{3}$$

In the low-intensity limit case, the electron displacement in the laser field is much less than λ_0 ($k_0\Delta \ll 1$) and does not significantly affect the radiation. All harmonics are in the specular direction with respect to the incident light. On the other hand, in the relativistic regime, the factor $k_0\hat{\boldsymbol{n}}\cdot\boldsymbol{x}$ in Eq. (1) becomes important since the electron displacement is now comparable to λ_0, where high harmonics peaked at directions apart from that of incidence are efficiently generated.

Figure 2 shows the angular dependence of K_n for the first to the 50th (from right to left) harmonics of laser frequency for $a_0 = 3$. One sees that in the nonlinear radiation from a single relativistic electron, a considerable part of the radiated energy is in the higher harmonics. Radiation at the fundamental laser frequency is comparatively intense, but it has a wide angular spread and peaks at the normal of the electron orbit. With increasing harmonic order, the angular distribution of the harmonics is shifted towards the direction of the electron motion, together with increasingly sharper peaks. The radiation at the higher harmonics is confined to a narrow cone in the direction of motion, an effect that results directly from the relativistic displacement Δ of the electron in the laser field.

To analyze the influence of the grating structure on the high-harmonic emission pattern, we neglect the influence of the tooth edges on the current distribution as well as the

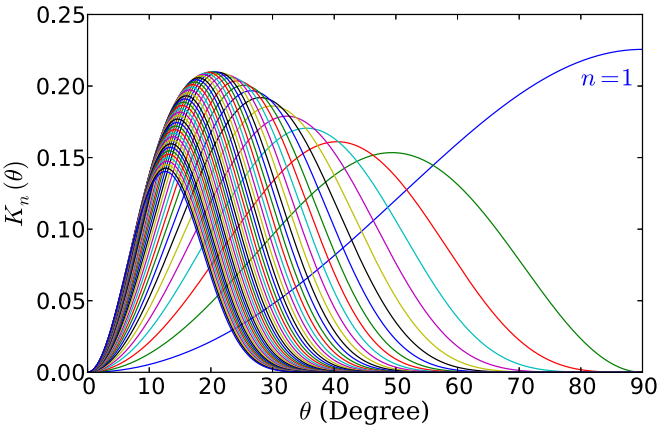

FIG. 2. The angular distribution of K_n, or the contribution of a single quivering electron to the emitted radiation, for $n = 1$ to 50 (right to left) and $a_0 = 3$.

interrelation between each tooth. Then the current density on the grating surface can be rewritten as the sum of the currents in each tooth [15]:

$$\vec{\mathbf{J}}_{\text{total}}(\boldsymbol{x},t) = \sum_{m=1}^{L/\ell} \vec{j}(y - m\ell, t), \tag{4}$$

where L is the effective grating length inside the laser spot. Thus, the radiated power per unit solid angle of the nth harmonic due to whole current can be expressed as

$$\frac{dP_n}{d\Omega} = \left(\frac{\gamma m_e \omega_0 c}{2\pi e}\right)^2 F_n(\omega_0,\theta) K_n(\theta), \tag{5}$$

where

$$F_n(\omega_0,\theta) = \left|\sum_{m=1}^{L/\ell} e^{-imn\ell k_0\cos\theta}\right|^2 = \frac{\sin^2(n\omega_0 L\cos\theta/2c)}{\sin^2(n\omega_0\ell\cos\theta/2c)} \tag{6}$$

is the factor of the interference. For a large number of teeth inside the laser spot ($L \gg \ell$), we obtain

$$F_n(\omega_0,\theta) \to \sum_{m\neq 0} \frac{n\omega_0 L}{|m|\ell}\delta(n\omega_0 - \omega_m). \tag{7}$$

In this case, the relationship between the grating spacing and the angles of the interference radiation is governed by the grating equation [15]

$$\omega_m = \frac{2\pi|m|c}{\ell\cos\theta}, \tag{8}$$

where m is the harmonic mode of the grating periodicity.

The term F_n denotes the contribution from the periodic grating on the harmonic radiation source. It acts as a frequency modulator to enhance or suppress the specific harmonics at particular observation angle. The match condition of enhancement is $\omega_m = n\omega_0$ (where m is an integer), which means the wavelength of the harmonic is the order of the grating periodicity. The typical modulation introduced by the grating is shown in Fig. 3(a). For harmonic numbers $n \neq \lambda_0/\ell$ ($n = 1$ to 3), F_n peaks sharply at 90° and decreases rapidly as the angle decreases. However, for harmonic number $n = \lambda_0/\ell$ ($n = 4$), the peak of F_n are spread flatly in the range $0° \to\sim 10°$. As can be seen in Fig. 3(b), such a flat distribution is typical of the $n = m\lambda_0/\ell$ harmonic, with the spread angle decreasing slightly with the increase of the harmonic number. Obviously, when a large number of harmonics are produced by the quiver electrons, harmonics satisfying $\lambda_0/n = \ell/m$ can be effectively enhanced and folded into this flat emission angle. On the other hand, several isolated peaks of harmonic also appear at large angles. Being very sharp and not overlappeing with each other, only a small amount of harmonic energy could be converged in those directions.

The HHG radiation power from a solid plasma grating is determined by the parameters K_n and F_n. Here K_n depicts the strong radiation from a single electron bunch, while F_n takes into account the interference effect of periodic grating on the emitted radiation. Since both K_1 and F_1 peak at $\theta = 90°$, the power at the fundamental frequency is concentrated in the direct backscattering direction. For the higher harmonics, however, the peaks of K_n and F_n do not coincide, so the corresponding radiation is concentrated at different angles

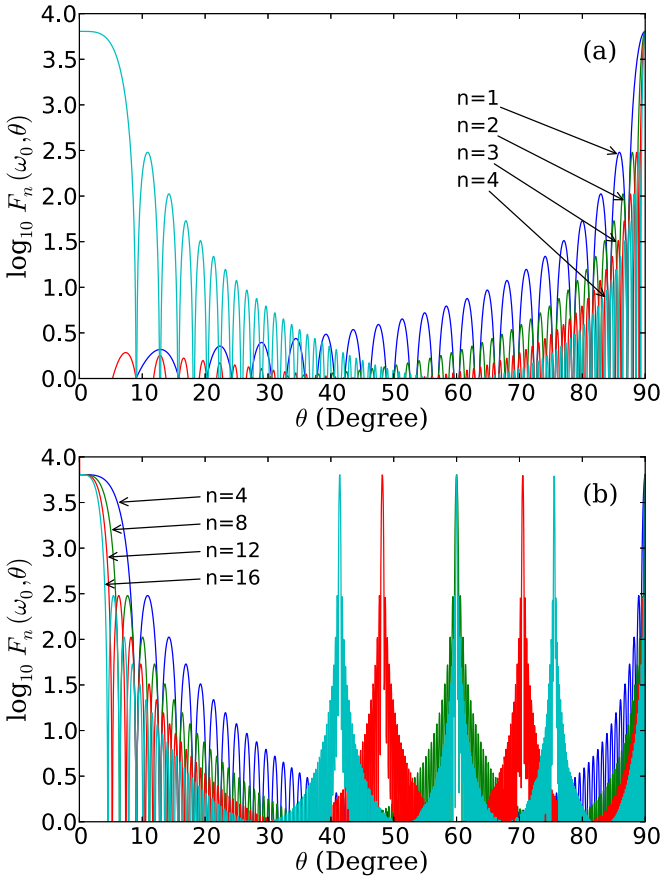

FIG. 3. The interference parameter F_n for the harmonics (a) $n = 1$ to 4 and (b) $n = 4$ to 16. Here, the tooth gap and grating length are $\ell = \lambda_0/4$ and $L = 20\lambda_0$, respectively.

away from the normal. Figure 4 shows the angular distribution from the $n = 4$ to 16th laser harmonics (or $m = 1$ to 4th harmonics of the grating periodicity). As we can see, the power of the radiation matching the harmonics of the grating periodicity are peaked at small angles with respect to surface direction and they decrease rapidly as the angle increases. Moreover, both the angle and its angular spread of each harmonic decrease slightly with the harmonic number.

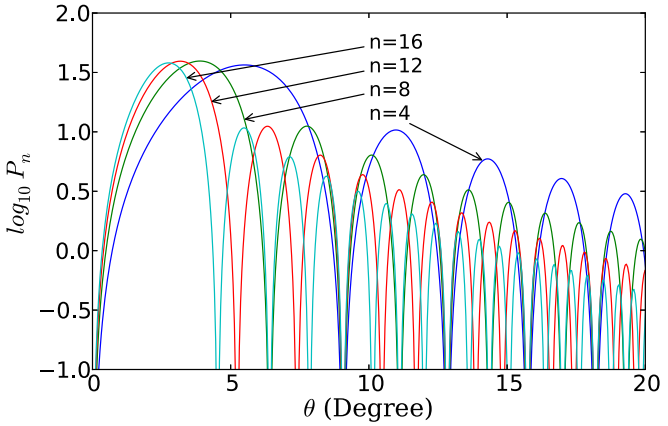

FIG. 4. The angular distribution of P_n for $a_0 = 3$, giving the relative radiation power of the $n = 4 \rightarrow 16$ harmonics from a grating surface. The parameters of the grating is same as Fig. 3.

To check the validity of above analytical model, HHG from the interaction of a relativistic laser pulse with a plasma grating is also numerically studied by using the two-dimensional relativistic and electromagnetic PIC code PDLPICC2D [16,17]. A linearly polarized laser pulse of Gaussian spatial profile is normally incident from the left onto the center of a plasma grating. The temporal profile of the laser pulse is $a = a_0 \sin^2(\pi t/\tau)$, where $\tau = 10\tau_0$ and τ_0 is the laser period. The diameter of the focus spot is $6.0\lambda_0$. The laser intensity a_0 is 3.0, corresponding to $I_0\lambda_0^2 \sim 1\times10^{19}$ W cm^{-2} μm^2. The plasma grating target is of size $6\lambda_0$ width and $2\lambda_0$ thickness and has a toothy structure on its left surface. The width w and height h of each tooth is $\lambda_0/16$ and $\lambda_0/8$, respectively. The periodicity of the teeth is $\ell = \lambda_0/4$, which is considerably less than the laser wavelength. This precludes resonant surface plasmon excitation, which requires a near wavelength periodicity $2/3 \leqslant \ell/\lambda_0 \leqslant 1$ [18,19]. The plasma is of initial density $n_0 = 20n_c$. Considering $\lambda_0 = 2\pi c/\omega_0 =$ 800 nm, this corresponds to a laser with ≈120 mJ, a spot size of 4.8 μm, and $\tau = 27$ fs interacting with a plasma grating with $n_0 = 2.75\times10^{22}$ cm^{-3}.

As shown in Figs. 5(a)–5(c), the linearly polarized incident laser pulse is mirror reflected by the grating surface without noticeable distortion. The intense harmonics radiation of p-polarization, propagating in the $\pm y$ directions along the

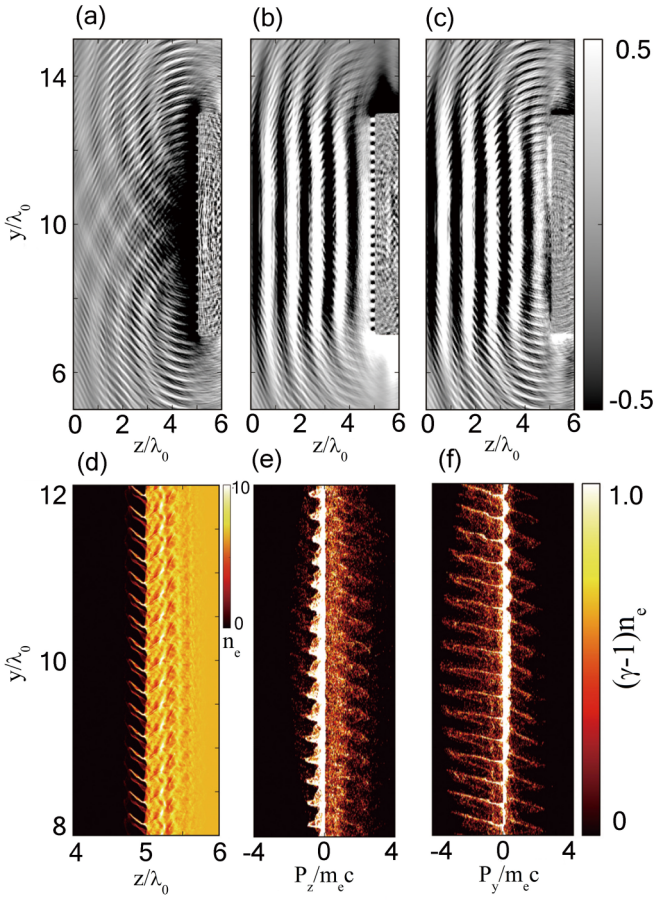

FIG. 5. Snapshot of radiation field components (a) E_z, (b) E_y, and (c) B_x at $t = 14\tau_0$. (d) Electron density distribution and phase spaces (e) (y, P_z) and (f) (y, P_y) at $t = 8\tau_0$. E and B are normalized by $m_e\omega_0 c/e$ and n_e is normalized by n_c.

surface in narrow solid angles, is effectively generated. Very weak harmonics with intensity more than one order of magnitude lower and propagating in a larger angle can also be observed. Driven by the laser field, the relativistic electrons from the teeth oscillate along the grating surface as a chain of bunches. The transverse momentum p_y is ~ 3 [in Fig. 5(f)], roughly equal to the laser intensity. The instantaneous location of the oscillating electron [in Fig. 5(d)] is obviously deviated from the initial position. As indicated by our model, it is significant for high-order harmonic generation. The longitudinal momentum of electrons driven by the laser ponderomotive force $p_z \sim 1$ [in Fig. 5(e)], essential for HHG in the flat plasma case, is not significant in this case. Due to the interference effect of grating, HHG in the specular direction is obviously suppressed in the simulation.

Figure 6(a) shows the temporal structure of the radiated pulse at $\theta \sim 5^\circ$. From the inset, one can see that a single pulse is of short duration, $\sim 0.1\tau_0 = 270$ as, and the interval between the pulses is only $\sim 0.3\tau_0 = 810$ as. As such HHG is mainly from the acceleration of electrons under the laser fields, the entire emission pulse lasts $\sim 10\tau_0$, with the spatial profile similar to the driving laser pulse. The corresponding HHG radiation spectrum is shown in Fig. 6(b). A characteristic feature is that only harmonics at $4\omega_0$, $8\omega_0$, $12\omega_0$, ..., up to $40\omega_0$, show up, which supports our analytical prediction that only the harmonics of the grating periodicity can be emitted under angles close to the grating surface. The angular distributions of three intense harmonics are shown in Fig. 6(c). The 4th harmonic peaks at $\theta \sim 5^\circ$ with a solid angle spread of $\Omega < 10^\circ$ is consistent with the numerical result given in Fig. 4. Moreover, it can be seen that both the angle and its spread decrease slightly with an increase of the harmonic number.

This technique of harmonic generation mentioned above works well only if the driven laser pulse has a very high contrast. The prepulses, typical of chirped pulse amplification laser systems, can lead to early plasma formation and destruction of surface structures before the main pulse. Fortunately, techniques such as using a plasma mirror to achieve ultrahigh pulse-to-prepulse contrast ratios now offer the opportunity to carry out such experimental studies at very high intensity. The typical periodic structure of tens to hundreds of nanometes for the HHG experiments now can be easily manufactured at low cost by mechanical processing. If needed, high-repetition HHG radiation can also be realized by using a cylindrical shell target with a grating surface and motor-controlled rotation, so a new surface can be placed into the laser spot position after each shot.

In conclusion, we have investigated HHG from a relativistic intensity laser beam normally incident on a solid plasma grating by analytical modeling and PIC simulation. It shows that the emission at high harmonics of the grating periodicity is strongly enhanced, which propagates along the grating surface direction with a narrow solid angle. This radiation originates from the broad-frequency radiation emitted by the oscillating relativistic electron bunches in the laser field. Then it is further strongly modulated and amplified by the interference effect of the grating. The emitted radiation is in the form of coherent attosecond pulse trains. Such radiation pulses are useful for diagnostics of the structural properties and the corresponding electron dynamics in material surfaces [20].

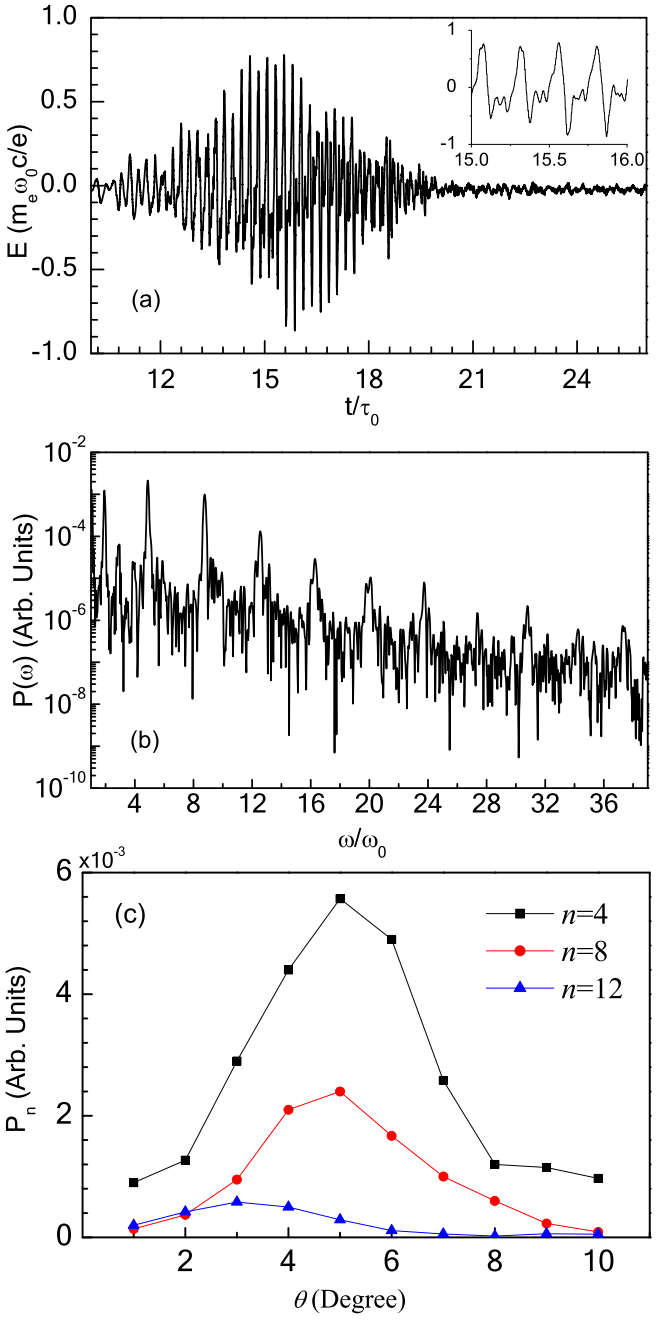

FIG. 6. (a) Temporal profile of the normalized radiation fields at $\theta \sim 5^\circ$ and (b) the corresponding spectrum. (c) Angular distribution of the intensity of three harmonics from the grating surface. The inset in (a) shows the a magnified segment of the structure of the generated attosecond radiation pulse.

This work was supported by the National Basic Research Program of China (Grant No. 2013CBA01504), the National Natural Science Foundation of China (Grants No. 11475259, No. 11175253, No. 11374262, and No. 91230205), the Research Program of NUDT, and the Open Fund of the State Key Laboratory of High Field Laser Physics (SIOM). We thank the Guangzhou National Supercomputing Center for providing their computing facilities.

[1] M. Hentschel, R. Kienberger, C. Spielmann, G. A. Reider, N. Milosevic, T. Brabec, P. Corkum, U. Heinzmann, M. Drescher, and F. Krausz, Nature **414**, 509 (2001).
[2] R. Kienberger *et al.*, Nature **427**, 817 (2004).
[3] E. Goulielmakis *et al.*, Science **305**, 1267 (2004).
[4] F. Krausz and M. Ivanov, Rev. Mod. Phys. **81**, 163 (2009).
[5] M. Uiberacker *et al.*, Nature **446**, 627 (2007).
[6] A. L. Cavalieri *et al.*, Nature **449**, 1029 (2007).
[7] U. Teubner, K. Eidmann, U. Wagner, U. Andiel, F. Pisani, G. D. Tsakiris, K. Witte, J. Meyer-ter-Vehn, T. Schlegel, and E. Forster, Phys. Rev. Lett. **92**, 185001 (2004).
[8] S. V. Bulanov, N. M. Naumova, and F. Pegoraro, Phys. Plasmas **1**, 745 (1994).
[9] M. Behmke, D. an der Brügge, C. Rödel, M. Cerchez, D. Hemmers, M. Heyer, O. Jäckel, M. Kübel, G. G. Paulus, G. Pretzler, A. Pukhov, M. Toncian, T. Toncian, and O. Willi, Phys. Rev. Lett. **106**, 185002 (2011).
[10] M. Cerchez, A. L. Giesecke, C. Peth, M. Toncian, B. Albertazzi, J. Fuchs, O. Willi, and T. Toncian, Phys. Rev. Lett. **110**, 065003 (2013).
[11] X. Lavocat-Dubuis and J.-P. Matte, Phys. Rev. E **80**, 055401(R) (2009).
[12] X. Lavocat-Dubuis and J.-P. Matte, Phys. Plasmas **17**, 093105 (2010).
[13] J. D. Jackson, *Classical Electrodynamics* (Wiley, New York, 1975).
[14] W. Yu, M. Y. Yu, J. Zhang, and Z. Xu, Phys. Rev. E **57**, R2531 (1998).
[15] J. H. Brownell, J. Walsh, and G. Doucas, Phys. Rev. E **57**, 1075 (1998).
[16] H. B. Zhuo, Z. L. Chen, W. Yu, Z. M. Sheng, M. Y. Yu, Z. Jin, and R. Kodama, Phys. Rev. Lett. **105**, 065003 (2010).
[17] H. B. Zhuo, Z. L. Chen, Z. M. Sheng, M. Chen, T. Yabuuchi, M. Tampo, M. Y. Yu, X. H. Yang, C. T. Zhou, K. A. Tanaka, J. Zhang, and R. Kodama, Phys. Rev. Lett. **112**, 215003 (2014).
[18] S. Kahaly, S. K. Yadav, W. M. Wang, S. Sengupta, Z. M. Sheng, A. Das, P. K. Kaw, and G. R. Kumar, Phys. Rev. Lett. **101**, 145001 (2008).
[19] M. Raynaud, J. Kupersztych, C. Riconda, J. C. Adam, and A. Heron, Phys. Plasmas **14**, 092702 (2007).
[20] G. A. Mourou, T. Tajima, and S. V. Bulanov, Rev. Mod. Phys. **78**, 309 (2006).